Dynamic Self-Loops in Networks of Passive and Active Binary Elements

Paul Baconnier,[1] Margot H. Teunisse,[1,2] and Martin van Hecke[1,2]
[1]AMOLF, 1098 XG Amsterdam, The Netherlands
[2]Huygens-Kamerlingh Onnes Laboratory, Leiden University, 2300 RA Leiden, The Netherlands

(Received 8 January 2025; revised 14 July 2025; accepted 22 October 2025; published 13 November 2025)

Models of coupled binary elements capture memory effects in complex dissipative materials, such as transient responses or sequential computing, when their interactions are chosen appropriately. However, for random interactions, self-loops—cyclic transition sequences incompatible with dissipative dynamics—dominate the response and undermine statistical approaches. Here we reveal that self-loops originate from energy injection and limit cycles in the underlying physical system. We, furthermore, introduce interaction ensembles that strongly suppress or completely eliminate self-loops, allowing statistical studies of memory in large dissipative systems. Our Letter opens a route toward a unified description of passive and active multistable materials using hysteron models.

DOI: 10.1103/x1b1-rynn

Sequences of transitions between metastable states govern the hysteresis [1], memory [2–9], emergent computing [10–12], sequential shape morphing [13,14], and adaptive behavior [15,16] of driven dissipative materials, such as crumpled sheets, disordered media, and metamaterials [9] [Fig. 1(a)]. As these states are often composed of local, two-state elements, with or without hysteresis, the response is commonly described by models of interacting hysterons or binary spins at zero temperature [Fig. 1(b)]. While models without interactions are well understood [1,17–19], interactions are crucial for capturing complex responses such as avalanches, transient responses, and multiperiodic cycles [5,20]. Pairwise interactions are captured by a matrix c_{ij} which represents how element i's flipping thresholds are influenced by element j [Fig. 1(c)]. In some cases, c_{ij} can be measured [7,10], and for networks of physical bistable elements, it can be modeled [12,21–25]. Hysteron models with appropriate interactions then enable accurate predictions of the systems response and memory effects [5,8,10,12,25–27].

Yet, the precise interactions are often unknown, or the goal is to understand system classes rather than a single experiment. Strikingly, assigning random interaction coefficients [4,5,20,30–32] overwhelmingly produces self-loops [Fig. 1(d)]: avalanches that get trapped in a repeating sequence of states that never settle [20,33–36]. Such dynamic loops—prohibited in dissipative systems—can be avoided by using symmetric interactions ($c_{ij} = c_{ji}$), as commonly done in spin glasses where asymmetry implies energy input and oscillations [33–42]. However, for hysteretic binary elements, whose strong nonlinearity invalidates Maxwell-Betti reciprocity [43], asymmetric interactions are compatible with dissipation. For example, a small ridge i may weakly affect a larger one j but not vice versa: $|c_{ij}| < |c_{ji}|$ [Fig. 1(c)]. Such asymmetric interactions are experimentally observed and theoretically modeled [10,12,25] and are crucial for explaining memory effects [5,32]. A conundrum thus arises: though physical and essential, random asymmetric interactions yield unphysical self-loops.

Here we uncover the mechanism that generates self-loops and show that their probability approaches 1 in large systems of asymmetrically coupled hysterons. We discuss physical networks with active bistable elements, map them to interacting hysterons, and show that these produce self-loops linked to limit cycles in the networks: rather

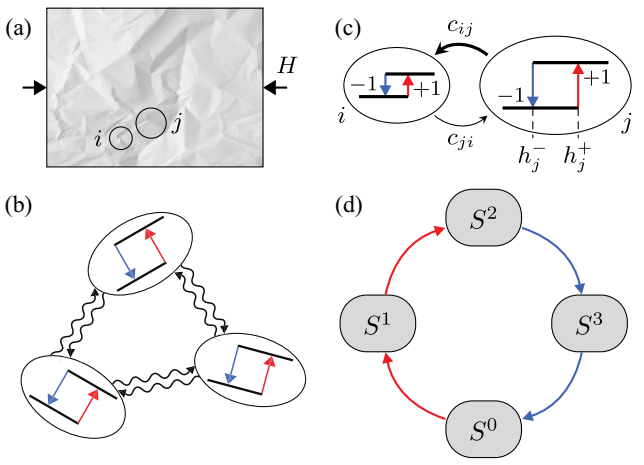

FIG. 1. (a) Crumpled sheet with bistable elements (ridges i and j) [7]. (b) Abstract hysteron models employ interacting binary elements. (c) Variations in strength of physical elements map to asymmetric hysteron interactions ($|c_{ij}| > |c_{ji}|$). (d) Self-loop in a (partial) transition graph. When the switching thresholds satisfy $H^+(S^1) < H^+(S^0)$, $H^-(S^2) > H^+(S^0)$, and $H^-(S^3) > H^+(S^0)$ and the system is in state S^0, increasing the driving H above its threshold $H^+(S^0)$ triggers a self-loop, as all states are unstable [28].

than being unphysical, self-loops reveal that coupled hysteron models span passive and active physical systems. Surprisingly, active elements may give rise to symmetric hysteron interactions. Finally, we introduce weakly asymmetric interaction ensembles to suppress self-loops, develop strict ensembles to eliminate them, and use these to study avalanche statistics and cyclic response in large hysteron systems. Our Letter uncovers subtle relations between the symmetry of hysteron interactions, self-loops, and physical energy injection. Moreover, it shows that hysteron models unify the description of passive and active multistable materials, connects the self-loop sector to limit cycles in active systems, and enables statistical studies of memory effects and pathways in dissipative and mixed systems.

Model—We consider N binary elements, $s_i = \pm 1$, which form collective states $S = (s_1, s_2, \ldots)$. The system is driven by a global field H, and the stability range of each element i in state S is given by switching thresholds $H_i^{\pm}(S)$. For pairwise interactions,

$$H_i^{\pm}(S) = h_i^{\pm} - \sum_{j \neq i} c_{ij} s_j, \tag{1}$$

where $h_i^{\pm}$ are the bare switching thresholds of element i. To model spins, we take $h_i^{+} = h_i^{-}$, whereas for hysterons, $h_i^{+} > h_i^{-}$ [1,18,19]. The matrix c_{ij}, with $c_{ii} = 0$, encodes cooperative ($c_{ij} > 0$) or frustrated ($c_{ij} < 0$) interactions that may be asymmetric ($c_{ij} \neq c_{ji}$) [5,12,25,27].

In this model, each state S has a range of stability, encoded in state switching thresholds $H^{\pm}(S)$ that follow from the extrema of $H_i^{\pm}(S)$: $H^{+}(S) \coloneqq \min_{i^-}[H_i^{+}(S)]$ and $H^{-}(S) \coloneqq \max_{i^+}[H_i^{-}(S)]$, where $i^{\pm}$ are the indices where $s_i = \pm 1$. When the system is in state S^0 and H is increased above $H^{+}(S^0)$ or decreased below $H^{-}(S^0)$, state S^0 loses stability and its unstable hysteron flips. Depending on n_u, the number of unstable hysterons in the resulting state S^1, three different scenarios arise [20,31]. When $n_u = 0$, state S^1 is stable; when $n_u = 1$, state S^1 is unstable and its unstable hysteron flips; when $n_u > 1$, multiple hysterons are unstable. The latter case, which is abundant in large systems [28], leads to a race condition and requires a dynamical rule to specify the next step in the transition [10,12,20,27,31]. In the remainder, we flip the most unstable element first [5]; this rule is physically plausible and corresponds to the zero-temperature limit of the Glauber dynamics [44,45] [for other rules see Supplemental Material [28]].

Hysterons with symmetric interactions—Although hysteron interactions are not expected to be symmetric, numerical sampling reveals that symmetric interactions consistently avoid self-loops. This can be proven by showing that the quantity $V(S)$, written as

$$V(S) = -\sum_{i^{\mp}} \left[s_i (H - h_i^{\pm}) + \frac{1}{2} \sum_{j \neq i} c_{ij} s_i s_j \right], \tag{2}$$

is a Lyapunov-like function of the system, which guarantees that the latter always converges toward a stable state and thus prohibits self-loops (Appendix A).

Random asymmetric coupling: Gaps and self-loops—We now exploit random interactions, where c_{ij} and c_{ji} are sampled independently. For any value of H, each isolated element has one stable phase or two within the hysteretic range. Without interactions, stable states can thus be easily formed by combining stable elements. However, interactions make the switching thresholds dependent on the collective state, effectively randomizing stability ranges and creating gaps, ranges of H where no state is stable.

We find two related scenarios where interactions lead to self-loops. The length of a self-loop, i.e., the number of unstable states visited within the cycle, is denoted L. We consider state S going unstable by the driving crossing a critical value H^c. In the first scenario, H^c lies at the edge of a gap, and the system gets inevitably trapped in a self-loop as there are no stable states. In the second, a set of L distinct unstable states transition toward each other, forming a periodic attractor, and the system gets trapped, despite the presence of other stable states at $H = H^c$.

To investigate the statistics of gaps, self-loops, and the self-loop size distribution [28], we sample the model using an event-driven algorithm [5]. We consider collections of hysterons with thresholds in a compact range [5,8,32]: we flatly sample the midpoints of the bare switching thresholds $h_i^c = (h_i^{+} + h_i^{-})/2$ from the interval $[-1, 1]$ and the interaction coefficients c_{ij} from $[-J_0, J_0]$. Unless noted otherwise, we flatly sample the spans $\sigma_i = h_i^{+} - h_i^{-} > 0$ from [0, 0.5].

We find that the probability P_g^0 of a gap, meaning the absence of a stable state at $H = 0$, and the fraction of gaps f_G both increase as power laws when $NJ_0 \ll 1$ [Figs. 2(a) and 2(b)]. For $NJ_0 \gg 1$, they saturate at significant values. The probability that states have a finite stability range decreases exponentially with N: for large N, stable states become rare, prohibiting statistical studies of transitions [28].

Gaps imply self-loops, but self-loops can also occur outside of gaps. Therefore, the probability of a self-loop occurring starting from a random state at $H = 0$, P_{sl}^0, is larger than the corresponding gap probability P_g^0 [Fig. 2(c) and Supplemental Material [28]]. Similarly, we calculated the total probability of observing a self-loop at any value of H, P_{sl}, by starting from every stable state, increasing and decreasing H, and checking whether the ensuing transitions yield at least one self-loop. We find that P_{sl} approaches 1 in large, strongly coupled systems [Fig. 2(d) and [28]]. This dominance of self-loops is robust; hysterons with fixed spans $\sigma_i = 0.5$ and binary spins where $\sigma_i = 0$ also have $P_{\mathrm{sl}} \to 1$ in the large coupling limit [28,33–36]. Hence, self-loops, incompatible with the dissipative systems we aim to model, are unavoidable for random interactions, and for large systems completely overwhelm the response.

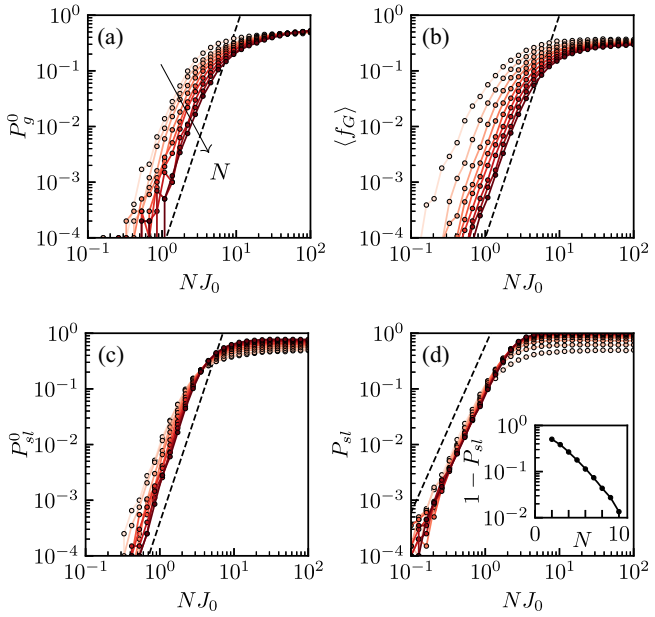

FIG. 2. Statistical measures for gaps and self-loops scale when plotted as function of NJ_0 (10^5 samples; color from light to dark as N increases from 2 to 10). (a) Probability P_g^0 of finding a gap at $H = 0$ (dashed line indicates slope 4). (b) Averaged fraction of gaps f_G, where f_G is defined as the ratio of the size of intervals where no stable states exist divided by $H^-(++\ldots) - H^+(--\ldots)$ (dashed line indicates slope 4). (c) Probability P_{sl}^0 of finding at least one self-loop at $H = 0$ (dashed line indicates slope 4). (d) Probability P_{sl} of finding at least one self-loop for any value of H (dashed line indicates slope 3). Inset: the probability to be self-loop-free, $1 - P_{\mathrm{sl}}$, decays to zero exponentially with N for large couplings ($NJ_0 = 10^2$).

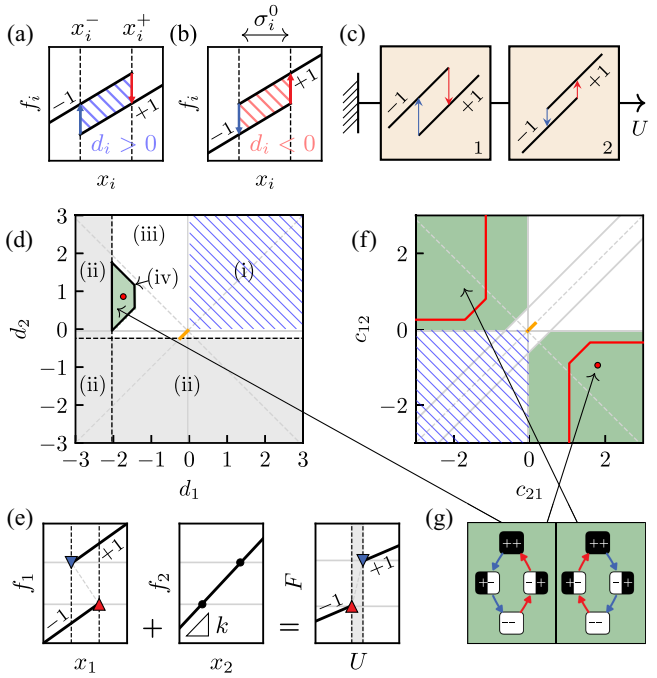

FIG. 3. Self-loops in networks containing active elements. (a), (b) Force-displacement curves for a dissipative element with $d_i > 0$ and $\Delta E_i < 0$ [(a), blue], and for an active element with $d_i < 0$ and $\Delta E_i > 0$ [(b), red]. (c) Two serially coupled elements, with total displacement $U = x_1 + x_2$. (d) Four classes of behaviors for two serially coupled elements as function of d_1 and d_2; here $(x_1^-, x_1^+) = (-1, 1)$, $(x_2^-, x_2^+) = (0.2, 0.4)$. (e) Serially coupling one active element and a linear spring (representing one of the elastic branches of the second element) can produce a gap without stable states $[U^+(\triangle) < U^-(\triangledown)]$ if d_1 is strongly negative [28]. (f) Regions where self-loops emerge for two coupled hysterons; for fixed $\sigma_1 = \sigma_2 = 0$ (green areas) and for (σ_1, σ_2) determined for the physical system represented by the red dot in (d) (red boundaries). The blue hatched regions in (d),(f) represent purely dissipative systems. Orange lines in (d),(f) indicate active elements that lead to symmetric hysteron interactions. (g) Two $L = 4$ self-loops observed in (d),(f).

Networks of active elements—To gain further insights into the emergence of self-loops in physical systems, we consider networks of bilinear, hysteretic springs,

$$f_i(x_i) = x_i - d_i s_i, \qquad \Delta E_i := 2 d_i \sigma_i^0, \tag{3}$$

where transitions occur at $x_i = x_i^{\pm}$, $\sigma_i^0 := x_i^+ - x_i^-$ is taken positive, and ΔE_i is the dissipated energy per hysteresis loop [Figs. 3(a) and 3(b)]. Once the geometry of the network and the parameters of all elements are specified, the network can be mapped to an interacting hysteron model [12,25]. This mapping never yields hysteron parameters that produce self-loops as long as the physical elements dissipate energy, i.e., when $d_i > 0$.

We find that networks that include active elements ($d_i < 0$), enabled by, e.g., force-generating components activated when $s_i = 1$ [Fig. 3(b)], are mapped to hysteron models that can feature self-loops. For simplicity, we consider a network of two serially coupled elements, where the mapping yields $c_{ij} = -d_j$ and $\sigma_i = 2(\sigma_i^0 + d_i)$ [12,25], producing four distinct behaviors [Figs. 3(c) and 3(d)]. (i) When both elements are passive, the hysteron spans σ_i are positive, the interaction coefficients are both negative, and no self-loops occur [12]. (ii) For strongly active elements, i.e., $d_i < -\sigma_i^0$, the hysteron spans σ_i become negative [Fig. 3(e)]. Here we expect the physical system to feature dynamic limit cycles [46–48], (partly) captured by an extended hysteron model. (iii) Weakly active elements map to hysterons with $\sigma_i > 0$ and interaction coefficients not accessible with passive elements. Strikingly, active elements with $d_1 = d_2 < 0$ map to hysteron models with symmetric interactions [Figs. 3(d) and 3(f), orange line]: there is no simple relation between the symmetry of c_{ij} and energy input. (iv) Crucially, for appropriately chosen activity, the physical system maps to the hysteron model with an $L = 4$ self-loop. For details, see Supplemental Material [28].

Hence, active elements extend the range of realizable hysteron parameters, may produce negative hysteron spans,

and allow one to access the hysteron sector with self-loops. Similar mechanisms also arise in fully dynamic models combining activity and bistability [49]. While larger, more complex networks remain to be understood, our example shows that self-loops can be physically interpreted as arising from energy injection in networks of two-state elements. The hysteron model features self-loops because it encompasses both passive and active systems.

Proliferation of self-loops—We now return to the hysteron model and seek to understand the parameters for which self-loops occur. Each self-loop is associated with a set of linear inequalities and occurs in a polytope in parameter space $(h_i^{\pm}, c_{ij})$ [5,20,31,32]. We first consider $L = 4$ loops [Fig. 3(g)]. For two spins, we find that a gap of size $|\Delta c| - |\Delta h^c|$ opens up when $c_{12}c_{21} < 0$ and $|\Delta c| > |\Delta h^c|$, where $\Delta c := c_{12} - c_{21}$ and $\Delta h^c := h_2^c - h_1^c$. These conditions are sufficient and necessary for the emergence of a self-loop [Fig. 3(f)]. For two hysterons, the range in parameter space where these self-loops can occur shrinks [Fig. 3(f) and [28]]. Finally, we can extend these conditions to arbitrary N; as only two elements i and j are involved for $L = 4$ self-loops, such short self-loops are prohibited by requiring $c_{ij}c_{ji} \geq 0$ for all pairs (i, j) [28].

By identifying all potential self-loops with $L \leq 2^N$, one could, in principle, determine all corresponding polytopes; the complement of their union is then free of self-loops. We have investigated the number of distinct self-loops, each corresponding to a different polytope in parameter space, with L. While our approach allows an efficient classification of the self-loop structures, we find that their number grows extremely rapidly with N (Appendix E and Supplemental Material [28]). This proliferation of the number, length, and complexity of self-loops makes deriving explicit and sharp conditions that identify all self-loops unfeasible. In the remainder, we first introduce a lenient strategy that removes the shortest and suppresses longer self-loops, followed by strict ensembles that fully eliminate all self-loops but are overly restrictive.

Lenient strategy: Weak asymmetry—We introduce the notion of weak asymmetry (WA): $c_{ij}c_{ji} \geq 0$ for all pairs (i, j). Not only does WA eliminate $L = 4$ self-loops, but it also suppresses the number of longer self-loops that are realizable (Appendix E and [28]). Statistical sampling reveals that WA is an effective strategy to suppress self-loops. In particular, $P_{\mathrm{sl}}^0 \to 0$ for large N, allowing one to sample individual transitions, although P_{sl} slowly grows with N: the combinatorial possibilities of finding a self-loop dominates in large systems [28]. Nevertheless, for intermediate N, WA strongly suppresses self-loops, e.g., $P_{\mathrm{sl}} \approx 14\%$ for large couplings and $N = 10$. Hence, WA strictly prohibits short self-loops and suppresses longer self-loops.

Strict ensembles—We now present ensembles of asymmetric interactions that strictly prohibit self-loops. First, if all interactions are positive $(c_{ij} \geq 0)$, avalanches exhibit monotonic evolution of the magnetization $m := \Sigma s_i$, thus prohibiting self-loops (Appendix B). If all interactions are negative, and either $c_{ik} = -d_k$ (constant columns) or $c_{ki} = -d_k$ (constant rows), where $d_k \geq 0$, self-loops are also prohibited. In the former case [which corresponds to the hashed blue region in Fig. 3(d)], the interactions prohibit scrambling [12], which, in turn, prohibits self-loops (Appendix C); in the latter case, the interactions only allow avalanches of length 2, too short to form a self-loop when $\sigma_i \geq 0$ (Appendix D and Supplemental Material [28]). We note that the statistics of, e.g., avalanches and self-loops drastically depends on the dynamical rule in all these ensembles. In particular, when race conditions are not allowed [12,20,31], constant-column interactions restrict the avalanche size $A \leq 2$, whereas flipping the most (or least) unstable elements leads to much larger A [Fig. 4(a)]. Moreover, flipping all unstable elements simultaneously instead of only the most unstable one leads to a dominance of $L = 2$ self-loops for symmetric, constant-column, and constant-row interactions [28].

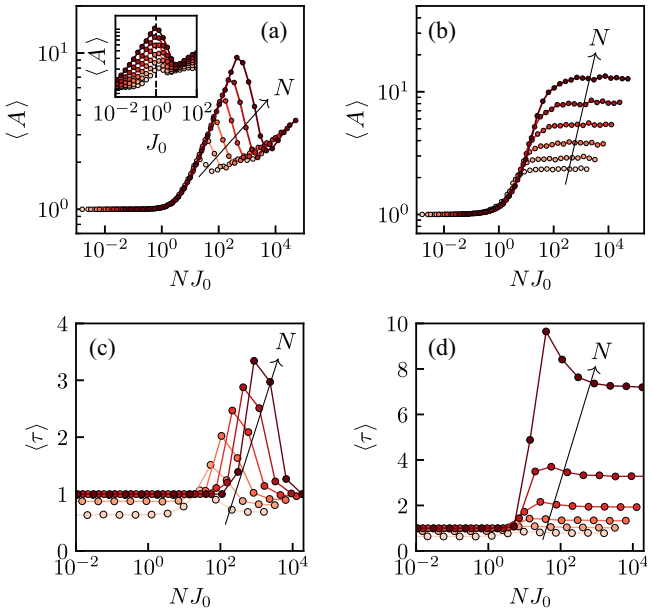

FIG. 4. Simulations of large systems of coupled hysterons in the constant columns (left) and symmetric (right) ensembles ($N = 16, 32, \ldots, 512$ for increasingly dark colors). (a),(b) Ensemble averaged avalanche size $\langle A \rangle$. To determine these, we initialize the system at a stable state S^0 at $H = 0$, increase H, and measure the number of flips before the system settles on a stable state. (c),(d) Ensemble averaged transient $\langle \tau \rangle$, where τ is the number of cyclic drive cycles after which the system reaches a periodic orbit [28].

The strictly self-loop-free ensembles allow us to study the statistics of unprecedentedly large systems of interacting hysterons, including the distributions of avalanche sizes A, transient times τ, and multiperiodicities T of orbits under cyclic drive (Fig. 4 and Supplemental Material [28]). We find that these significantly depend on the ensemble, e.g.,

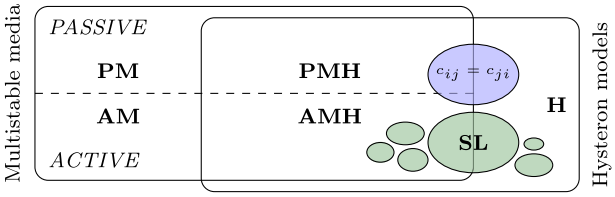

FIG. 5. Relations between active and passive multistable physical systems, hysteron models, self-loops, and symmetry of c_{ij}. Both active and passive systems can map to hysteron models with symmetric couplings ($c_{ij} = c_{ji}$, blue region); in this case, self-loops are forbidden. The region where self-loops occur forms a complex cloud of polytopes in the space of hysteron models (SL, green regions).

avalanches and transients are shorter in the constant columns than in the symmetric ensemble, and their dependence on NJ_0 is qualitatively different.

Conclusion and outlook—The picture that emerges is that hysteron models connect with both passive and active multistable physical systems. We summarize the relations between networks of bistable elements, the symmetry of hysteron interactions, and self-loops in Fig. 5. Strikingly, symmetric hysteron interactions can arise from networks of active or passive bistable elements, but cannot feature self-loops, and asymmetric hysteron interactions may lead to self-loops, but there is no simple criterion to delineate the parameter regions where self-loops can emerge. Future challenges first concern expanding the range of mappings between physical networks and hysterons, to define additional self-loop-free hysteron ensembles and to extend the hysteron model with a measure of energy dissipation. Second, recent works have studied the emergence of oscillatory dynamics through nonreciprocal interactions [41,42,50,51], and our explorations suggest that nonreciprocally coupled passive bistable elements may be amenable to a hysteronlike description. Third, since dynamical effects [52] or geometric nonlinearities [25] lead to transitions not described by current hysteron models, even for passive physical systems (PM), it will be exciting to explore the interplay between dynamics, geometry, and bistability for active systems (AM). Fourth, we suggest that self-loops can be linked to multiperiodic responses under cyclic driving using the concept of transition scaffold [5,31]. Finally, it is an open question whether all sectors of the interacting hysteron model are realizable with physical systems (H).

Acknowledgments—We thank Dor Shohat, Yoav Lahini, Corentin Coulais, Jonas Veenstra, and Menachem Stern for valuable discussions and an anonymous referee for astute criticism. P. B., M. H. T., and M. v. H. acknowledge funding from European Research Council Grant No. ERC-101019474.

Data availability—The data that support the findings of this article are openly available [53].

[1] F. Preisach, Z. Phys. **94**, 277 (1935).
[2] N. C. Keim, J. D. Paulsen, Z. Zeravcic, S. Sastry, and S. R. Nagel, Rev. Mod. Phys. **91**, 035002 (2019).
[3] J. D. Paulsen and N. C. Keim, Proc. R. Soc. A **475**, 20180874 (2019).
[4] C. W. Lindeman and S. R. Nagel, Sci. Adv. **7**, eabg7133 (2021).
[5] N. C. Keim and J. D. Paulsen, Sci. Adv. **7**, eabg7685 (2021).
[6] T. Jules, A. Reid, K. E. Daniels, M. Mungan, and F. Lechenault, Phys. Rev. Res. **4**, 013128 (2022).
[7] D. Shohat, D. Hexner, and Y. Lahini, Proc. Natl. Acad. Sci. U.S.A. **119**, e2200028119 (2022).
[8] N. C. Keim and D. Medina, Sci. Adv. **8**, eabo1614 (2022).
[9] J. D. Paulsen and N. C. Keim, Annu. Rev. Condens. Matter Phys. **16**, 61 (2024).
[10] H. Bense and M. van Hecke, Proc. Natl. Acad. Sci. U.S.A. **118**, e2111436118 (2021).
[11] L. J. Kwakernaak and M. van Hecke, Phys. Rev. Lett. **130**, 268204 (2023).
[12] J. Liu, M. Teunisse, G. Korovin, I. R. Vermaire, L. Jin, H. Bense, and M. van Hecke, Proc. Natl. Acad. Sci. U.S.A. **121**, e2308414121 (2024).
[13] D. Melancon, A. E. Forte, L. M. Kamp, B. Gorissen, and K. Bertoldi, Adv. Funct. Mater. **32**, 2201891 (2022).
[14] A. Meeussen and M. van Hecke, Nature (London) **621**, 516 (2023).
[15] L. M. Kamp, M. Zanaty, A. Zareei, B. Gorissen, R. J. Wood, and K. Bertoldi, Proc. Natl. Acad. Sci. U.S.A. **122**, e2508310122, (2025).
[16] J. Veenstra, C. Scheibner, M. Brandenbourger, J. Binysh, A. Souslov, V. Vitelli, and C. Coulais, Nature (London) **639**, 935 (2025).
[17] M. Mungan, S. Sastry, K. Dahmen, and I. Regev, Phys. Rev. Lett. **123**, 178002 (2019).
[18] M. Mungan and M. M. Terzi, in *Annales Henri Poincaré*, Vol. 20 (Springer, New York, 2019), pp. 2819–2872.
[19] M. M. Terzi and M. Mungan, Phys. Rev. E **102**, 012122 (2020).
[20] M. van Hecke, Phys. Rev. E **104**, 054608 (2021).
[21] G. Puglisi and L. Truskinovsky, J. Mech. Phys. Solids **48**, 1 (2000).
[22] A. Nicolas, E. E. Ferrero, K. Martens, and J.-L. Barrat, Rev. Mod. Phys. **90**, 045006 (2018).
[23] D. Kumar, S. Patinet, C. E. Maloney, I. Regev, D. Vandembroucq, and M. Mungan, J. Chem. Phys. **157**, 174504 (2022).
[24] D. Kumar, M. Mungan, S. Patinet, and D. Vandembroucq, Phys. Rev. E **112**, 035411 (2025).
[25] D. Shohat and M. van Hecke, Phys. Rev. Lett. **134**, 188201 (2025).
[26] J. Ding and M. van Hecke, J. Chem. Phys. **156**, 204902 (2022).
[27] J. D. Paulsen, arXiv:2409.07726.
[28] See Supplemental Material at http://link.aps.org/supplemental/10.1103/x1b1-rynn for additional figures and simulation details, which includes Ref. [29].
[29] P. Ducarme, B. Weber, M. van Hecke, and J. T. Overvelde, Proc. Natl. Acad. Sci. U.S.A. **122**, e2423301122 (2025).
[30] N. C. Keim, J. Hass, B. Kroger, and D. Wieker, Phys. Rev. Res. **2**, 012004(R) (2020).
[31] M. Teunisse and M. van Hecke, R. Soc. Open Sci. **12**, 250753 (2025).

[32] C. W. Lindeman, T. R. Jalowiec, and N. C. Keim, Sci. Adv. **11**, eadr5933 (2025).
[33] H. Gutfreund, J. Reger, and A. Young, J. Phys. A **21**, 2775 (1988).
[34] K. Nutzel and U. Krey, J. Phys. A **26**, L591 (1993).
[35] H. Eissfeller and M. Opper, Phys. Rev. E **50**, 709 (1994).
[36] S. Hwang, V. Folli, E. Lanza, G. Parisi, G. Ruocco, and F. Zamponi, J. Stat. Mech. (2019) P053402.
[37] S. Kirkpatrick and D. Sherrington, Phys. Rev. B **17**, 4384 (1978).
[38] J. J. Hopfield, Proc. Natl. Acad. Sci. U.S.A. **79**, 2554 (1982).
[39] A. Crisanti and H. Sompolinsky, Phys. Rev. A **36**, 4922 (1987).
[40] D. Panchenko, *The Sherrington-Kirkpatrick Model* (Springer Science & Business Media, New York, 2013).
[41] M. Fruchart, R. Hanai, P. B. Littlewood, and V. Vitelli, Nature (London) **592**, 363 (2021).
[42] G. G. Lorenzana, A. Altieri, G. Biroli, M. Fruchart, and V. Vitelli, Phys. Rev. Lett. **135**, 187402 (2025).
[43] C. Coulais, D. Sounas, and A. Alu, Nature (London) **542**, 461 (2017).
[44] G. Parisi, Fractals **11**, 161 (2003).
[45] M. B. Jesi, *Spin Glasses: Criticality and Energy Landscapes* (Springer, New York, 2016).
[46] H. Xia, J. Wu, J. Zheng, J. Zhang, and Z. Wang, Lab Chip **21**, 1241 (2021).
[47] T. Sarkar, K. Lieberth, A. Pavlou, T. Frank, V. Mailaender, I. McCulloch, P. W. Blom, F. Torricelli, and P. Gkoupidenis, Natl. Electron. Rev. **5**, 774 (2022).
[48] P. Belleri, J. Pons i Tarrés, I. McCulloch, P. W. Blom, Z. M. Kovács-Vajna, P. Gkoupidenis, and F. Torricelli, Nat. Commun. **15**, 5350 (2024).
[49] J. Veenstra, O. Gamayun, X. Guo, A. Sarvi, C. V. Meinersen, and C. Coulais, Nature (London) **627**, 528 (2024).
[50] Y. Avni, M. Fruchart, D. Martin, D. Seara, and V. Vitelli, Phys. Rev. E **111**, 034124 (2025).
[51] Y. Avni, M. Fruchart, D. Martin, D. Seara, and V. Vitelli, Phys. Rev. Lett. **134**, 117103 (2025).
[52] L. Jin and M. van Hecke, arXiv:2507.02387.
[53] P. Baconnier, M. H. Teunisse, and M. van Hecke, Zenodo, https://zenodo.org/records/17475496 (2025).
[54] D. J. C. MacKay, *Information Theory, Inference, and Learning Algorithms* (Cambridge University Press, Cambridge, England, 2003).
[55] J. P. Sethna, K. Dahmen, S. Kartha, J. A. Krumhansl, B. W. Roberts, and J. D. Shore, Phys. Rev. Lett. **70**, 3347 (1993).
[56] D. E. Knuth, in *The Art of Computer Programming: Fundamental Algorithms* (Addison-Wesley, Reading, Massachusetts, 1975), pp. 634–634.
[57] M. Deza and R. Shklyar, arXiv:1003.4391.

End Matter

Appendix A: Systematic convergence for symmetric interactions—Here we show that symmetric interactions yield transitions than lower a Lyapunov-like function, first focusing on spins (for which $h_i^+ = h_i^- = h_i^c$) following standard approaches [38,54] and then extending the result to hysterons. Consider an initial state S^0 and a value of the drive H such that element p is unstable, which implies (i) $H > h_p^c - \sum_{j\neq p} c_{pj} s_j^0$, if $s_p^0 = -1$, and (ii) $H < h_p^c - \sum_{j\neq p} c_{pj} s_j^0$, if $s_p^0 = 1$, which can be rewritten as

$$s_p^0 \left(H - h_p^c + \sum_{j\neq p} c_{pj} s_j^0 \right) < 0. \tag{A1}$$

Let us now introduce the function V, reminiscent of a Sherrington-Kirkpatrick model with random thresholds,

$$\begin{aligned} V(\mathbf{s}) &= -\sum_i \left[s_i (H - h_i^c) + \frac{1}{2} \sum_{j\neq i} c_{ij} s_i s_j \right], \\ &= -\sum_i s_i (H - h_i^c) - \frac{1}{2} \sum_i \sum_{j\neq i} c_{ij} s_i s_j, \end{aligned} \tag{A2}$$

where the first and second term on the rhs of Eq. (A2) can be seen as a field and interaction term. We aim to compute $\Delta V = V(S^1) - V(S^0)$, where S^1 and S^0 are the state before and after snapping element p, i.e., $s_{i\neq p}^1 = s_{i\neq p}^0$ and $s_p^1 = -s_p^0$. Clearly, the terms with elements different than p will not contribute to ΔV, and by splitting the sums accordingly, we obtain

$$\begin{aligned} \Delta V = &-s_p^1 (H - h_p^c) + s_p^0 (H - h_p^c) \\ &- \frac{1}{2} \left(\sum_{i\neq p} c_{ip} s_i s_p^1 + \sum_{j\neq p} c_{pj} s_p^1 s_j - \sum_{i\neq p} c_{ip} s_i s_p^0 \right. \\ &\left. - \sum_{j\neq p} c_{pj} s_p^0 s_j \right), \end{aligned} \tag{A3}$$

which can be simplified to

$$\Delta V = 2 s_p^0 \left[(H - h_p^c) + \frac{1}{2} \sum_{j\neq p} (c_{jp} + c_{pj}) s_j \right], \tag{A4}$$

where we repeatedly use that, for $j \neq p$, $s_j^0 = s_j^1 =: s_j$. For the case of symmetric interactions, i.e., $c_{jp} = c_{pj}$, we find

$$\Delta V = 2 s_p^0 \left[(H - h_p^c) + \sum_{j\neq p} c_{pj} s_j \right]. \tag{A5}$$

Inserting the instability condition for element p, Eq. (A1) yields $\Delta V < 0$. Therefore, the function V is strictly decreasing for each single flip, which implies that the system cannot be trapped in a self-loop and must always evolve toward a stable state. Note the importance of the factor $1/2$ in Eq. (A2) in order to obtain the final result.

This demonstration can be extended to finite span hysterons, by explicitly making the distinction between hysterons with positive and negative phase and their respective thresholds, producing Eq. (2) of the main text.

Appendix B: Positive interactions—In this appendix, we show that, for positive (ferromagnetic) interactions, i.e., $c_{ij} \geq 0$, the system cannot get trapped into a self-loop. A self-loop is a cyclic avalanche: the system must come back to a previously visited unstable state. However, for positive interactions, each step in an avalanche "goes in the same direction," i.e., the magnetization $m \coloneqq \sum_i s_i$ evolves monotonically [20,55]. This prevents avalanches from revisiting earlier states, thus prohibiting self-loops, irrespective of the specific rule used to resolve race conditions [28].

Appendix C: Constant-column interactions—We now clarify why constant columns ($c_{ik} = -d_k$, $d_k \geq 0$) define a self-loop-free interaction ensemble. First, for negative (antiferromagnetic) interactions, avalanches (including self-loops) must be composed of alternating up-down transitions [20]. For $L \geq 6$, such self-loops exist [28]. However, all such self-loops violate loop return-point memory, which requires scrambling: the ordering of the switching thresholds must be state dependent [20]. Constant-column interactions do not allow for scrambling [12], therefore this ensemble strictly prevents all self-loops.

Appendix D: Constant-row interactions—We now show that in the constant-row ensemble ($c_{ki} = -d_k$, $d_k \geq 0$), avalanches consist of at most two hysteron flips, which is too short to allow self-loops. Without loss of generality, we consider an up avalanche initiated from state S^0 by an increase of H up to $H_p^+(S^0)$, triggering the flipping of hysteron p from $s_p = -1$ to $s_p = 1$ and leading to state S^1. Since we have negative interactions, avalanches must be composed of alternating up-down transitions, so that the next step would be the flipping of hysteron q from $s_q = 1$ to $s_q = -1$ leading to state S^2. To show that S^2 is stable to additional up flipping events, we first show that $H_i^+(S^0) = H_i^+(S^2)$ for $i \neq p, q$. Using that, in this ensemble $c_{ip} = c_{iq}$, and that $s_p^0 = -1$ and $s_q^0 = 1$, we find that

$$H_{i\neq p,q}^+(S^0) = h_i^+ - \sum_j c_{ij} s_j^0 \tag{D1}$$

$$= h_i^+ - \sum_{j\neq p.q} c_{ij} s_j^0 - c_{ip} s_p^0 - c_{iq} s_q^0 \tag{D2}$$

$$= h_i^+ - \sum_{j\neq p,q} c_{ij} s_j^0. \tag{D3}$$

Similarly, using that $s_p^2 = 1$ and $s_q^2 = -1$, we find that

$$H_{i\neq p,q}^+(S^2) = h_i^+ - \sum_{j\neq p,q} c_{ij} s_j^2, \tag{D4}$$

and as $s_{j\neq p,q}^2 = s_{j\neq p,q}^0$, we conclude that $H_i^+(S^0) = H_i^+(S^2)$ for $i \neq p, q$. Since in state S^0 all hysterons $i \neq p$, q are stable, they are also stable in state S^2. Moreover, both hysterons p and q are stable in state S^2 at $H = H_p^+(S^0)$: indeed, $H_p^-(S^2) = H_p^+(S^0) - \sigma_p - 2d_p < H_p^+(S^0)$, and hysteron q just flipped. Therefore, the longest possible avalanche in this interaction ensemble consists of two steps. By the same argument, this result also holds for other race conditions that involve flipping hysterons one by one [28].

Appendix E: Proliferation of self-loops—In this appendix, we focus on fundamental loops, which are defined as the unique loops that involve all elements ($n_e = N$) up to permutations of the element indices [i.e., the two $L = 4$ self-loops in Fig. 3(e) are equivalent]. We determine the potential number of fundamental loop structures, $M(n_e, L)$, from the combinatorics of flip sequences and calculate the number of realizable loops with pairwise interactions, $M_R(n_e, L)$ [28]. Both grow rapidly with n_e and L (Table I). In particular, for the shortest fundamental loops, $M(n_e, L = 2n_e)$ grows as $1, 6, 56, 796, \ldots$ for $n_e = 2, 3, 4, 5, \ldots$ [Figs. 3(b) and 3(c) for $n_e = 2, 3$], and our data suggest that each of these is realizable. The number of actual self-loops and polytopes grows even faster with N. Introducing n_e elements into a larger group of N elements, and including permutations, maps each fundamental loop to a significantly larger number of actual loops and polytopes, fueling a further combinatorial explosion. So while, in principle, we can identify the self-loops and for each determine their polytope in parameter space [31], in practice, this is not feasible.

TABLE I. Numbers of fundamental self-loops of size L involving n_e elements. Note that $4 \leq L \leq 2^N$ and $\log_2 L \leq n_e \leq L/2$, as each element undergoes an even number of flips; loops with n_e elements can visit at most 2^{n_e} states; and self-loops of size 2 are excluded by $h_i^+ \geq h_i^-$ [28]. The numbers in each box represent $M(n_e, L)$, $M_R(n_e, L)$, and $M_W(n_e, L)$, respectively. Note that the number of longest fundamental loops, $M(n_e, L = 2^{n_e})$, is given by the number of directed Hamiltonian cycles in the binary n_e cube $(1, 2, 112, 15109096, \ldots$ for $n_e = 2, 3, 4, 5, \ldots)$ [56,57].

L/n_e	2	3	4	5
4	1/1/0	⋯	⋯	⋯
6	⋯	6/6/2	⋯	⋯
8	⋯	2/0/0	56/56/24	⋯
10	⋯	⋯	176/114/4	796/796/376
12	⋯	⋯	420/145/1	9028/x/x
14	⋯	⋯	448/48/0	76640/x/x
16	⋯	⋯	112/4/0	535584/x/x